



Optimizing the Electrical Power in an Energy Harvesting System

Mattia Coccolo

*Nonlinear Dynamics, Chaos and Complex Systems Group,
Departamento de Física, Universidad Rey Juan Carlos,
Tulipán s/n, 28933 Móstoles, Madrid, Spain*

Grzegorz Litak

*Department of Applied Mechanics, Lublin University of Technology,
Nadbystrzycka 36, PL-20-618 Lublin, Poland*

Jesús M. Seoane and Miguel A. F. Sanjuán

*Nonlinear Dynamics, Chaos and Complex Systems Group,
Departamento de Física, Universidad Rey Juan Carlos,
Tulipán s/n, 28933 Móstoles, Madrid, Spain*

Received June 9, 2015

In this paper, we study the vibrational resonance (VR) phenomenon as a useful mechanism for energy harvesting purposes. A system, driven by a low frequency and a high frequency forcing, can give birth to the vibrational resonance phenomenon, when the two forcing amplitudes resonate and a maximum in amplitude is reached. We apply this idea to a bistable oscillator that can convert environmental kinetic energy into electrical energy, that is, an *energy harvester*. Normally, the VR phenomenon is studied in terms of the forcing amplitudes or of the frequencies, that are not always easy to adjust and change. Here, we study the VR generated by tuning another parameter that is possible to manipulate when the forcing values depend on the environmental conditions. We have investigated the dependence of the maximum response due to the VR for small and large variations in the forcing amplitudes and frequencies. Besides, we have plotted color coded figures in the space of the two forcing amplitudes, in which it is possible to appreciate different patterns in the electrical power generated by the system. These patterns provide useful information on the forcing amplitudes in order to produce the optimal electrical power.

Keywords: Nonlinear dynamics; optimization; vibrational resonance; energy harvesting.

1. Introduction

It is possible, all around us, to see small but powerful electrical devices greedy for energy. In fact, the performance of the electronic devices has increased rapidly along with their energy needs, while the capacity of the batteries has become suddenly inadequate [Paradiso & Starner, 2005]. Therefore, powering electronics devices without depending exclusively on the batteries, but by transforming the environmental energy into electrical energy,

has grown as an interesting open research field, called *energy harvesting*.

In this sense, mechanical vibrations are a possible and reliable energy source that can be exploited. In fact, different ideas have been proposed in order to transform environmental vibration kinetic energy into electrical energy, like using piezoelectric or electrostatic effects [Anton & Sodano, 2007; Arnold, 2007; Litak *et al.*, 2010], i.e. coupling a mechanical system as a source to a transduction mechanism.

Some numerical results [Gammaitoni *et al.*, 2009] have shown that the bistable energy harvesters are able to provide more energy in a frequency broadband than their linear counterparts, initially preferred [Roundy *et al.*, 2003]. It means that the nonlinear oscillators can exploit a wider spectrum of vibration frequencies, making them more adaptable and the best choice as shown in [Friswell *et al.*, 2011; Borowiec *et al.*, 2014; Haris *et al.*, 2014; Pellegrini *et al.*, 2012; Harne & Wang, 2013; Twiefel & Westermann, 2013].

In scientific literature it is usual to have the impression that all vibrations are detrimental because most publicized works discuss vibration reduction in one form or another. But since we are discussing about exploiting vibrations as a source of electrical energy, nonlinear environmental vibrations can be intentionally introduced into designs or enhanced in amplitude. The final objective is to take advantage of the benefits and then study by using mathematical tools for modeling and predicting the vibrational behaviors. Besides, it is important to state that vibrations are defined to be linear when the corresponding force of the potential is linear ($F = -kx$) and nonlinear otherwise. Therefore, we have decided to use nonlinear vibrations, not only because they are more general and realistic, but also because energy harvesters are supposed to be small enough to be contained into electronic devices. That means that even small vibration amplitudes result in large consideration within the system. Moreover, sometimes in kinetic energy harvesting systems, it can be useful to increment the effect of the vibrations in amplitude in order to produce more energy [Cocco *et al.*, 2014].

A phenomenon that can help to achieve this enhancement is the *vibrational resonance* (VR) [Landa & McClintock, 2000], where the resonance concept is the tendency of a system to oscillate with greater amplitude at some frequencies rather than at others. The VR phenomenon appears when a bistable system with a low (LF) and a high frequency (HF) forcing gives a response amplitude at the LF that grows until a maximum and then decreases, while we vary the amplitude of the HF forcing or the frequency. Other theoretical aspects of the VR have been developed in [Gitterman, 2001; Blekhan & Landa, 2004; Zaikin *et al.*, 2002]. The VR phenomenon can be explained as an amplification of the LF signal, due to a reduction of the stiffness of the system induced by the HF force. In other

words, it happens when the low frequency signal is able to induce cross-well transitions. So far, this phenomenon has been thoroughly studied in a large class of dynamical systems [Gandhimathi *et al.*, 2006; Daza *et al.*, 2013; Jayakumari *et al.*, 2009; Deng *et al.*, 2009; Rajasekar *et al.*, 2011], among others. In [Cocco *et al.*, 2014], we have studied the influence of this phenomenon on a Duffing oscillator driven by a bi-harmonic excitation, focusing our work on the effects of VR in harvesting systems. Following the same path, we have decided to study a bistable oscillator, studied in [Cottone *et al.*, 2009; Gammaitoni *et al.*, 2009; Vocca *et al.*, 2012] numerically and experimentally, driven by a HF and LF forcing, in which the double well potential is given by the repulsion of an external and an internal magnet situated as shown in Fig. 1. In this case, the two forcings simulate environmental vibrations and we analyze their interaction in order to exploit the VR phenomenon by tuning a different parameter value of Δ , which is the distance between the magnets (see Fig. 1). Accordingly, we have focused our attention on the power generated by the system by producing a two-dimensional map with an appropriate color code, that associates to every LF and HF forcing pair (F, f) a different color, that represents a value of the mean electrical power $\langle P \rangle$. As we will show later, different patterns can be visualized. To summarize, we will analyze the phenomenon of VR for different values of the distance between magnets Δ . Furthermore, we compute the electrical power generated for different frequencies and amplitudes of the forcing terms for various values of Δ .

This paper is organized as follows. In Sec. 2, we describe our prototype model, the bistable nonlinear oscillator which emulates our mechanical system. The phenomenon of the VR in our system and its implications in energy harvesting is described in Sec. 3. In Sec. 4, we study the response of the average power of the system in the vibrational resonance regime. A map of the electrical power response of the system is described in Sec. 5. A discussion and the main conclusions of this manuscript are presented in Sec. 6.

2. The Model

We have chosen for our study the mechanical system depicted in Fig. 1, which has been studied numerically and experimentally in [Cottone *et al.*, 2009; Gammaitoni *et al.*, 2009; Vocca *et al.*, 2012]. This

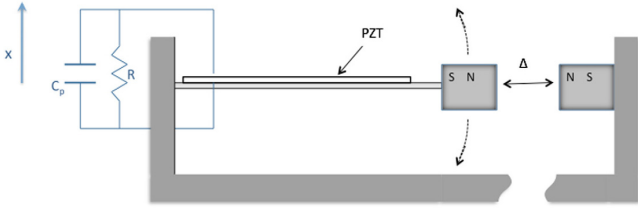


Fig. 1. The harvester considered has parameter Δ as the distance between the magnets, PZT the piezoelectric patch, R and C_p are the resistance and the capacitor of the coupled circuit, and the beam displacement is along x -axis.

system can be modeled as a bistable potential and the equation of motion reads as follows:

$$m\ddot{x} + \frac{dU(x)}{dx} + \gamma\dot{x} + K_v v(t) = F \cos(\omega t) + f \cos(\Omega t), \quad (1)$$

where $U(x)$ is the potential energy function of the cantilever with equivalent mass m , x is the vertical displacement around its mean value, the third term on the left $\gamma\dot{x}$, gives the energy dissipation due to the bending and in the fourth term we have $v(t)$, the voltage and K_v , the coupling constant of the piezoelectric sample, so that $K_v v(t)$ gives the energy transferred to the electric load R with the coupling equation:

$$\dot{v} + \frac{v(t)}{\tau_p} - \kappa_c \dot{x} = 0, \quad (2)$$

where κ_c is the position to voltage coupling coefficient. The time constant of the piezoelectric dynamics, τ_p , is related to the coupling capacitance C_p and to the resistive load R by $\tau_p = RC_p$. Finally, $F \cos(\omega t)$ and $f \cos(\Omega t)$ are the low frequency (LF) and the high frequency (HF) excitations, respectively. Notice that we have chosen for convenience $F \gg f$ as the respective forcing amplitudes, while $\omega = 0.5$ and Ω are the frequencies, that always have to satisfy the VR condition $\Omega \gg \omega$. The HF frequency value is $\Omega = 5$ if not indicated otherwise.

The potential energy function in Eq. (1) is given by:

$$U(x) = \frac{1}{2}K_{\text{eff}}x^2 + (ax^2 + b\Delta^2)^{-3/2}, \quad (3)$$

with K_{eff} , a and b represent constants related to the physical parameters of the cantilever. The parameter a is given by $a = d^2(\mu_0 M^2 / 2\pi d)^{-2/3}$ where μ_0 is the permeability constant, M the effective magnetic moment and $d = 2.97$ a geometrical parameter

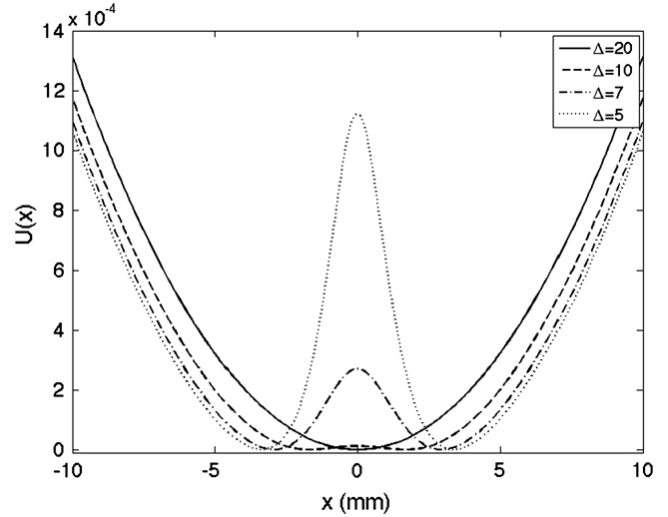


Fig. 2. Plot of the potential $U(x)$, given by Eq. (3), for different values of the distance between the magnets $\Delta = 0.005$, $\Delta = 0.007$, $\Delta = 0.010$ and $\Delta = 0.02$. The rest of the parameters are as shown in Table 1, in agreement with [Cottone *et al.*, 2009; Gammaitoni *et al.*, 2009; Vocca *et al.*, 2012]. All magnitudes follow the International System of units.

related to the distance between the measurement point and the cantilever length. The variable b is written as $b = a/d^2$. The tuning parameter Δ is used to move from a monostable potential to a bistable potential (see Fig. 2). In other words, it is the distance between the magnet on the top of the cantilever and the fixed magnet. Later, we will discuss the influence of this parameter on the electrical power harvested in the system of Eqs. (1)–(3). We start, from now on, every simulation from the initial condition $(x_0, y_0, v_0) = (0.001, 0, 0)$ ($y = \dot{x}$), using a Runge–Kutta integrator [Butcher, 1987] of fourth order. The parameter values used for the simulations are described in Table 1, according to [Cottone

Table 1. The simulations parameters.

Parameters	Description	Value
m	Cantilever equivalent mass	0.018 Kg
γ	Viscous parameter	0.022 kg/s
K_v	Piezoelectric coupling constant	0.0011 N/V
K_c	Position to voltage coupling coeff.	4.15×10^3 V/m
R_L	Load resistance	$300 \times 10^3 \Omega$
C	Piezoelectric capacitance	112×10^{-9} F
K_{eff}	Cantilever effective elastic constant	26.6 N/m
M	Effective magnetic moment	0.051 Am ²
μ_0	Magnetic permeability	$4\pi \times 10^{-7}$ H/m

et al., 2009; Gammaitoni et al., 2009; Vocca et al., 2012], where a comparison between the numerical simulations and an experimental apparatus has been done. We do not clarify the units other than in Table 1, because they do not change along the article. We have decided to study the harvester subjected to continuous vibrations for values of the amplitudes and frequencies sufficiently sensitive to a human being, as we can see in [Department of Environment and Conservation, 2006].

3. The Vibrational Resonance

The first step is the numerical study of the response of the system defined by Eqs. (1)–(3) for the displacement variable x , and the electrical power $P \propto V^2$, where V is the voltage generated by the system. When the system has a LF signal of amplitude F and frequency ω , and a HF signal of amplitude $f \ll F$ and frequency $\Omega \gg \omega$, the VR phenomenon can take place.

The usual procedure to search for VR is to compute, for different amplitudes f or frequency Ω [Landa & McClintock, 2000], the Q factor

$$Q = \frac{\sqrt{(C_s^2 + C_c^2)}}{F}, \quad (4)$$

where

$$C_s = \frac{2}{nT} \int_0^{nT} \Gamma(t) \sin(\omega t) dt \quad (5)$$

$$C_c = \frac{2}{nT} \int_0^{nT} \Gamma(t) \cos(\omega t) dt \quad (6)$$

and $\Gamma(t)$ is, in our case, the displacement x or the electrical power generated $P \propto V^2$, the number of

complete oscillations of the LF signal is n and $T = 2\pi/\omega$ is its period. The VR occurs, if it is possible to find a value of f or of Ω that maximizes the Q factor. This means that a particular value of the HF periodic signal has been found that optimizes the response of the system to the weak LF periodic signal. Here, we have explored a different scenario, where the values of the frequencies and forcing amplitudes are fixed by the environmental conditions and we modify only the parameter Δ .

3.1. Vibrational resonance for small variations in the forcing amplitudes and frequencies ratio

We have started our analysis with a value of the HF forcing amplitude $f = 0.1 \times 10^{-2}$ [as shown in Figs. 3(a) and 3(b)]. In these figures, the different curves related to different values of the LF forcing amplitude $0.1 \times 10^{-1} < F < 0.14 \times 10^{-1}$ show how the peaks detach around the value of $\Delta = 0.01$. The same behavior happens when we change the amount of the HF forcing amplitude $f = 0.5 \times 10^{-2}$ [see Figs. 3(c) and 3(d)], only a new peak detaches in the curve of $F = 0.011$ for a slightly larger Δ value. Also, we have computed the same curves for different amounts of frequency Ω , as shown in Figs. 4(a)–4(d). In Figs. 4(a) and 4(c) we can see that the peaks detach for the same Δ value. However, for a HF forcing value $f = 0.5 \times 10^{-2}$, as shown in Fig. 4(d), the Q factor for the electrical power Q_{v^2} shows a different behavior with respect to Q_x and another peak pops up for a slightly larger value of Δ . The analysis of the previous

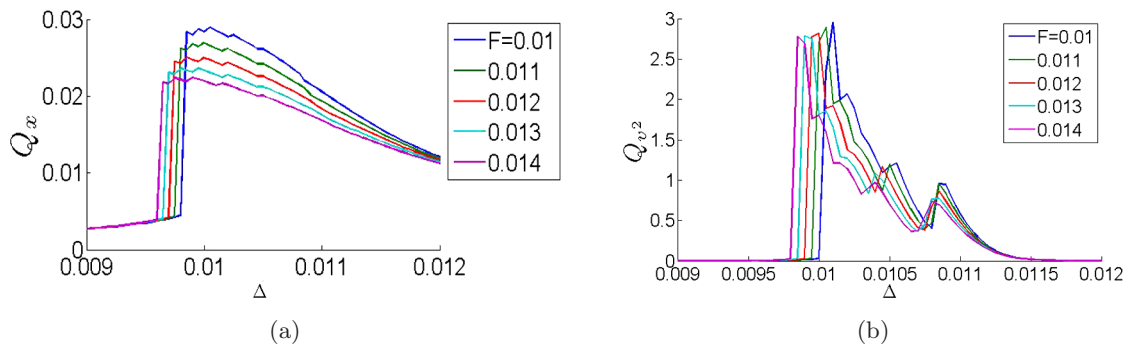


Fig. 3. Figures (a) and (c) plot Q_x versus Δ , for $f = 0.1 \times 10^{-2}$ and $f = 0.5 \times 10^{-2}$. Figures (b) and (d) plot Q_{v^2} versus Δ , for $f = 0.1 \times 10^{-2}$ and $f = 0.5 \times 10^{-2}$. All different curves are plotted for different values of F : $F = 0.11 \times 10^{-1}$, $F = 0.12 \times 10^{-1}$, $F = 0.13 \times 10^{-1}$, and $F = 0.14 \times 10^{-1}$. Note that there is a value of the Δ parameter that maximizes the Q factor, showing the occurrence of VR, although it shifts to smaller values when F value increases. In all these curves, we have used $(x_0, y_0, v_0) = (0.001, 0, 0)$ as the initial condition.

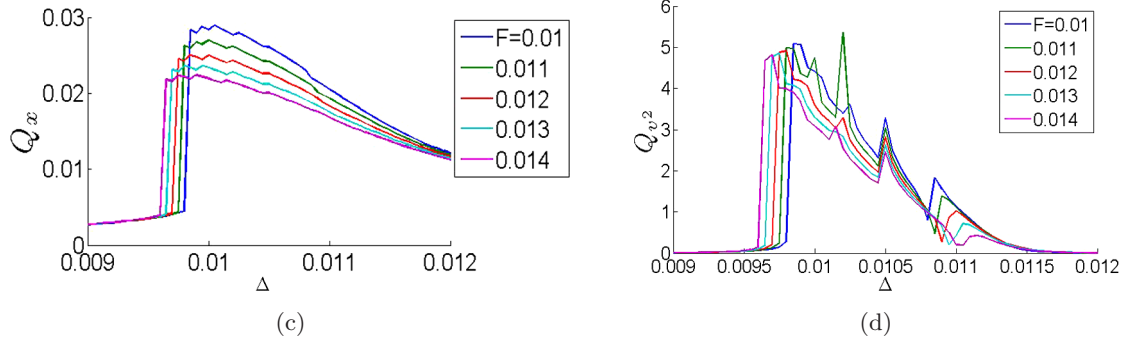


Fig. 3. (Continued)

figures shows us that a variation of the experimental parameter Δ can generate the VR phenomenon for which the role of the parameter f is crucial. In the situation in which VR exists, we have calculated the value of Δ for which we have a maximum in the average electrical power generated by the mechanical system, namely $\langle P \rangle \propto \langle V^2 \rangle$. This maximum can be observed in Fig. 5(a) where we show the values of

$\langle P \rangle$ for the case with $f = 0.1 \times 10^{-2}$. On the other hand, the average electrical power generated by the mechanical system, for the case with $f = 0.5 \times 10^{-2}$, is shown in Fig. 5(b), where qualitatively its behavior is the same as that in the case of the previous figure. We can see, as shown in Fig. 3, that the value of the parameter Δ for which the peaks are maximal coincides with the value for which the Q

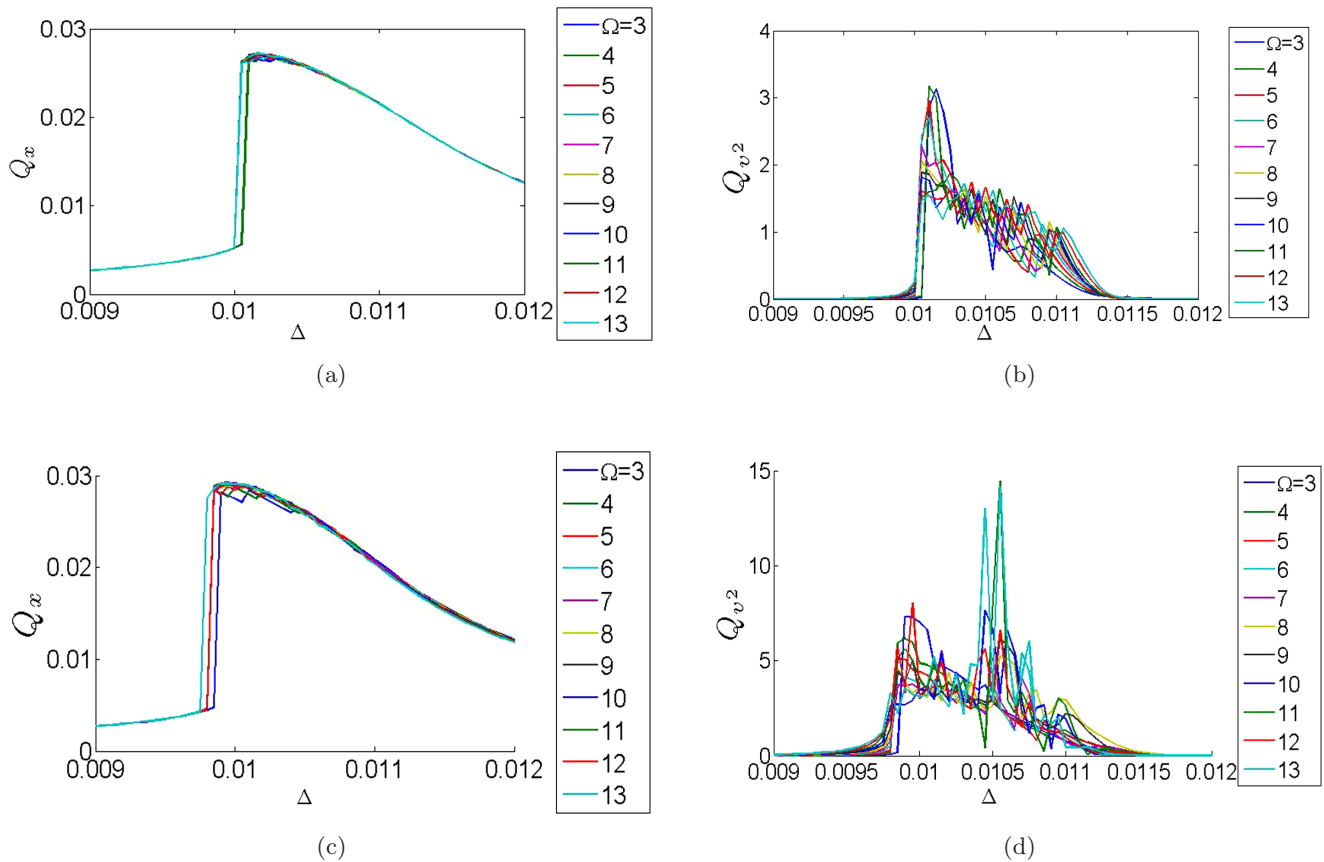


Fig. 4. Figures (a) and (c) plot the Q factor for the position, Q_x versus Δ , for $f = 0.1 \times 10^{-2}$ and $f = 0.5 \times 10^{-2}$. It is possible to see that in both figures the curves do not change significantly when the Ω value increases. Figures (b) and (d) plot the Q factor for the power Q_{v^2} versus Δ , for $f = 0.1 \times 10^{-2}$ and $f = 0.5 \times 10^{-2}$. Here, the scale changes and also the shape of the curves. Moreover, a new peak shows up in Fig. 4(d). All different curves are plotted for different values of the HF frequency Ω . In all these curves, we have used $(x_0, y_0, v_0) = (0.001, 0, 0)$ as the initial condition.

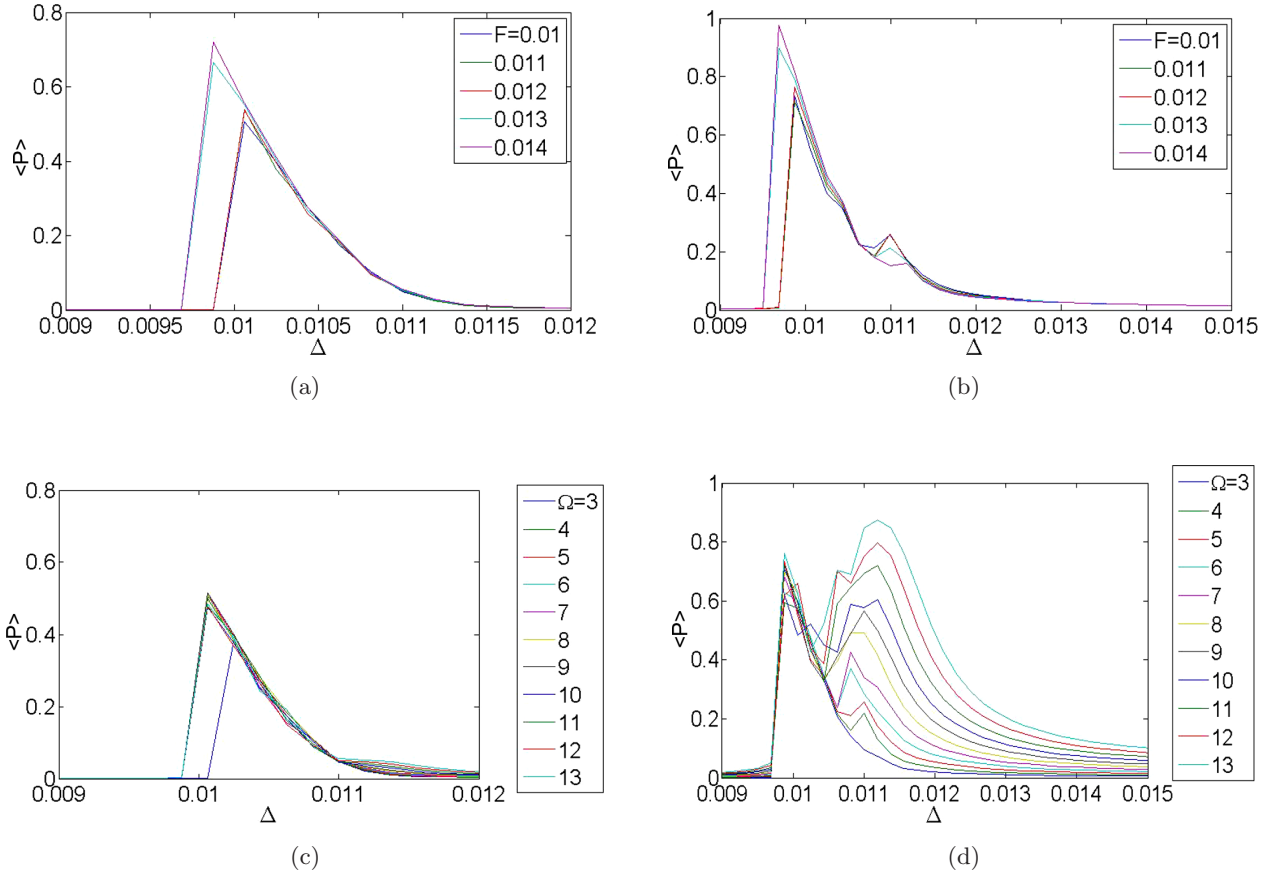


Fig. 5. Figures (a) and (b) plot the average electrical power, $\langle P \rangle \propto \langle V^2 \rangle$ versus Δ , for $f = 0.1 \times 10^{-2}$ and $f = 0.5 \times 10^{-2}$ for different values of F . Figures (c) and (d) plot the average electrical power $\langle P \rangle$ versus Δ , for $f = 0.1 \times 10^{-2}$ and $f = 0.5 \times 10^{-2}$ for different values of Ω . Figures (a)–(c) show a peak for the same Δ value, but figure (d) maximum is displaced with respect to the others and it is in agreement with Fig. 4(d). In all these curves, we have used $(x_0, y_0, v_0) = (0.001, 0, 0)$ as the initial condition.

factor is also maximum. The last figure, Fig. 5(d), shows us that the optimal distance Δ between the magnets for the VR to occur can depend on the LF forcing, in fact, a new maximum shows up while Ω is increasing.

3.2. Vibrational resonance for larger variations in the forcing amplitudes and frequencies ratio

In the previous subsection, we have shown that for a small difference of the amplitude F and the frequency Ω of the forcing, the peak of the VR occurs for almost the same Δ value. We have also shown that the maximum in electrical power and the peaks in the Q factor are related. In this subsection, we investigate the occurrence of the VR peak when the variation of the ratio between the two amplitudes and frequencies of the forcing is larger,

although the vibration values remain in a humanly acceptable scale. We study the possibility to establish that there are values of the Δ parameter that maximize the system response in electrical power for given environmental vibrations, even when the vibrational conditions vary on a larger scale. The Q factor for the displacement x and the electrical power $\langle P \rangle$ in the cases of different amplitudes F can be seen in Figs. 6(a)–6(d). In these figures, we have a similar behavior between them, insofar as the scale of F increases. On the other hand, in Figs. 7(a)–7(d), we have changed the frequency ratio, showing a strong change in the shape of the curves shown in Figs. 7(c) and 7(d) with respect to the ones shown in Figs. 7(a) and 7(b). In Figs. 8(a)–8(e) we attempt to clarify Fig. 7(d) by plotting in the different panels the shape of the curves for a shorter range of Ω . In these last figures, we can see that the peaks are localized in a narrow area of the figure, typically around the value $\Delta = 0.001$. When

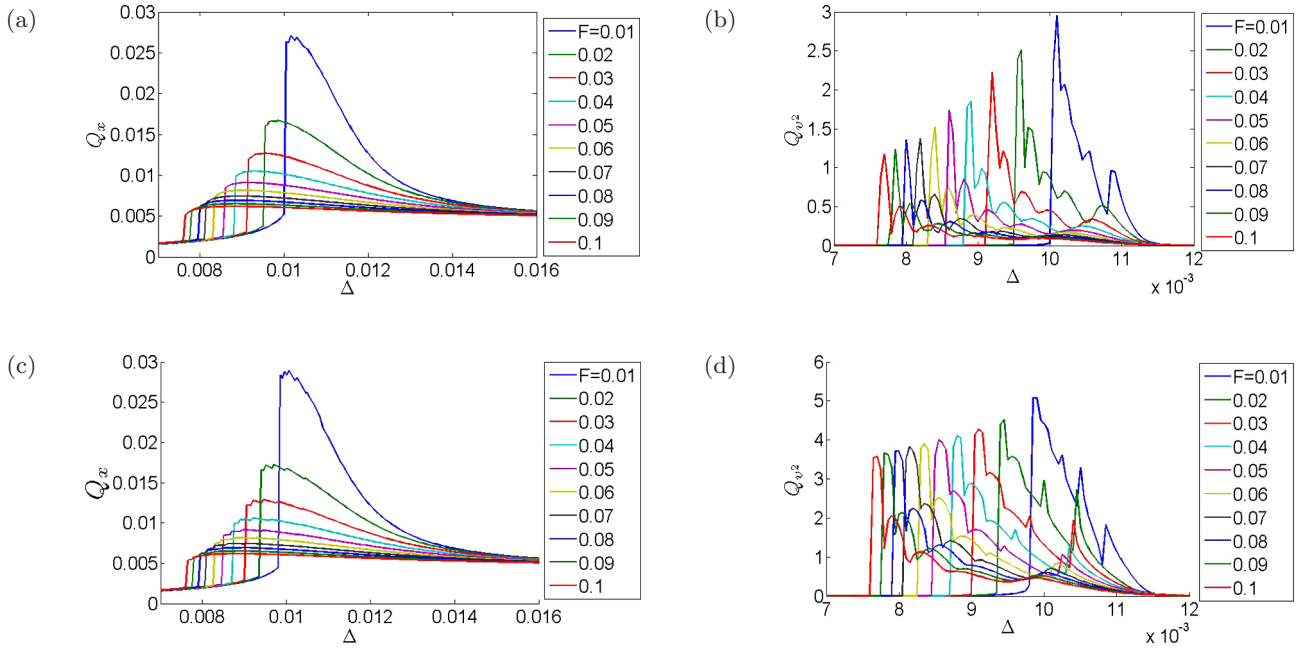


Fig. 6. Figures (a) and (c) plot the Q factor of the displacement Q_x versus Δ , for $f = 0.1 \times 10^{-2}$ and $f = 0.5 \times 10^{-2}$. Figures (b) and (d) plot the Q factor of the power Q_{v^2} versus Δ , for $f = 0.1 \times 10^{-2}$ and $f = 0.5 \times 10^{-2}$. All different curves are plotted for different values of F , larger with respect to Figs. 3(a)–3(d). The figures show that the peaks of both Q_x and Q_{v^2} shift as function of F value. In all these curves, we have used $(x_0, y_0, v_0) = (0.001, 0, 0)$ as the initial condition.

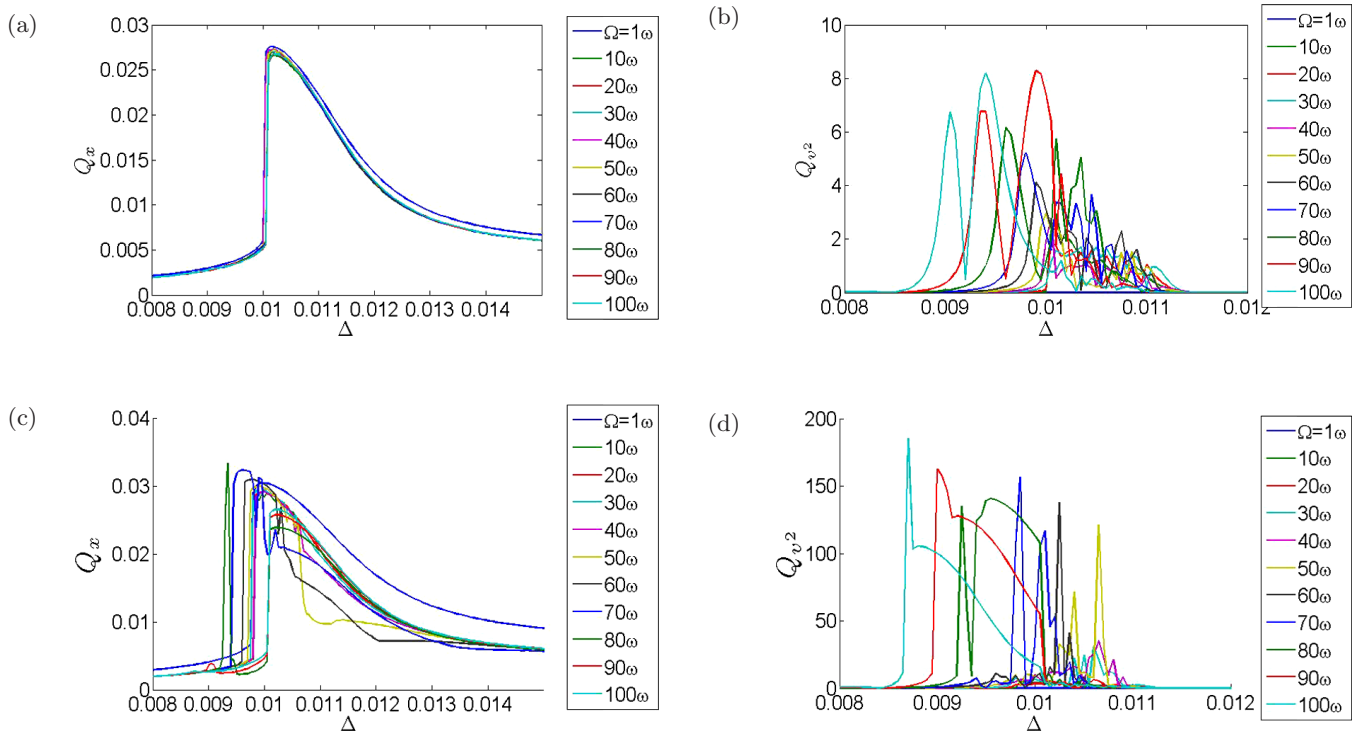


Fig. 7. Figures (a) and (c) plot the Q factor of the displacement Q_x versus Δ , for $f = 0.1 \times 10^{-2}$ and $f = 0.5 \times 10^{-2}$. Figures (b) and (d) plot the Q factor of the power Q_{v^2} versus Δ , for $f = 0.1 \times 10^{-2}$ and $f = 0.5 \times 10^{-2}$. All different curves are plotted for different values of HF frequency Ω , larger than Figs. 4(a)–4(d). The figures show that the peaks of both Q_x and Q_{v^2} show different behaviors. (d) For specific ranges of frequency Ω , we have used $(x_0, y_0, v_0) = (0.001, 0, 0)$ as the initial condition.

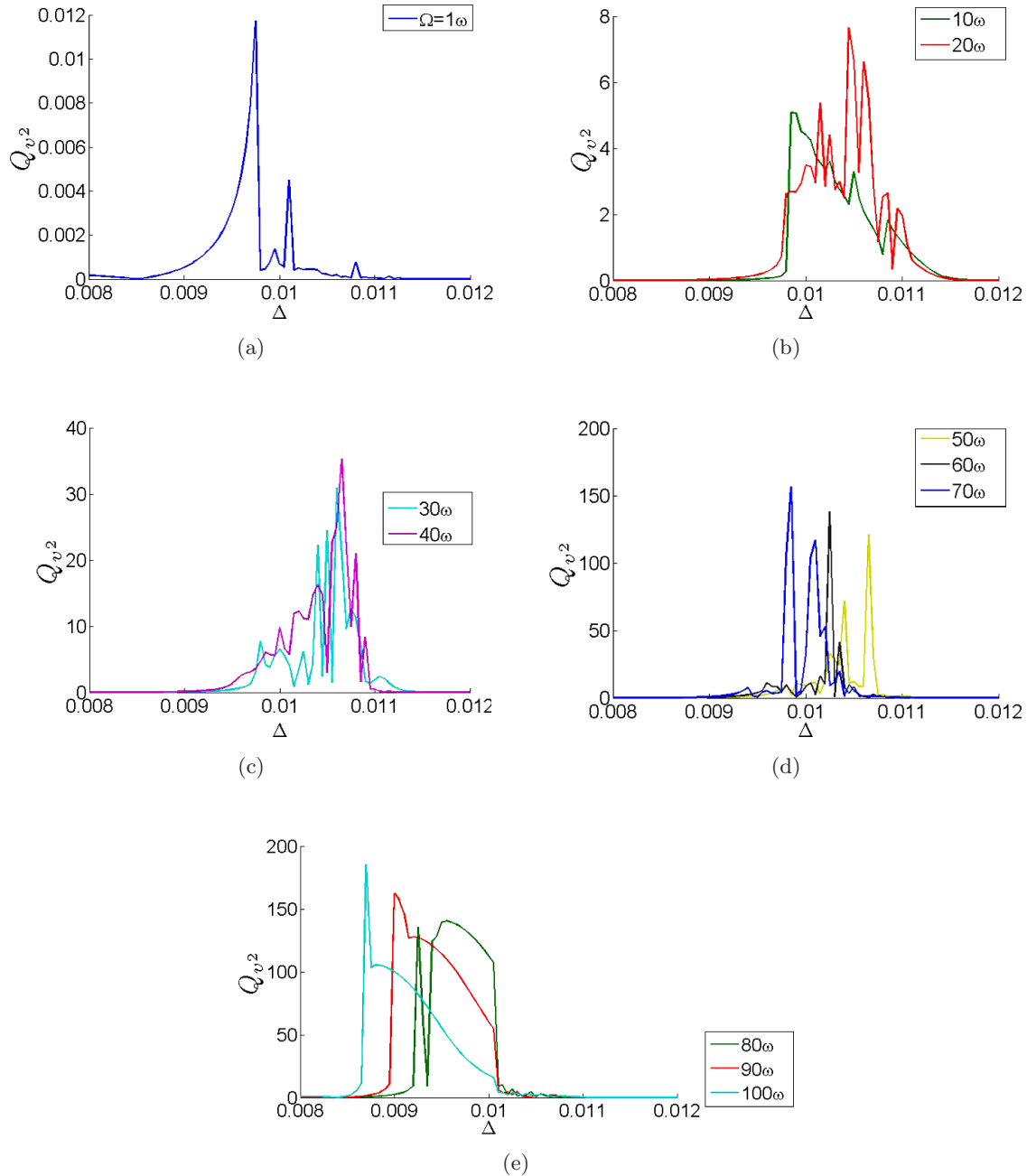


Fig. 8. Figures (a)–(e) plot the curves of Fig. 7(d) for a specific range of the frequency Ω . It is possible to appreciate that the scale changes abruptly from figures (c) to (d), but differently from Figs. 6(a)–6(d), the peaks are settled around the value $\Delta = 0.001$. To make the legend easier to read, the position of the Ω values match the ones of Fig. 7(d).

we study the average electrical power $\langle P \rangle$ shown in Figs. 9(a) and 9(b), we can see that the maximum electrical power follows the peak of the $Q_{v,2}$ as F increases, while otherwise in Figs. 9(c) and 9(d) it does not happen. In particular, we can appreciate besides the difference in scale, that the maxima in the electrical power are displaced with respect to the $Q_{v,2}$ shown in Fig. 7(d). To better visualize the curves of Figs. 9(c) and 9(d), we have split the two

figures into Figs. 10(a)–10(c) and Figs. 11(a)–11(d) respectively. Analyzing these figures, we can appreciate some similarity between them, in particular that for different values of Δ we have different maximal responses in electrical power depending on the HF frequencies Ω . An analysis of the figures from smaller to bigger Δ values can be fruitful. It is possible to see that just before the value $\Delta = 0.001$ the maximum is reached by the curve

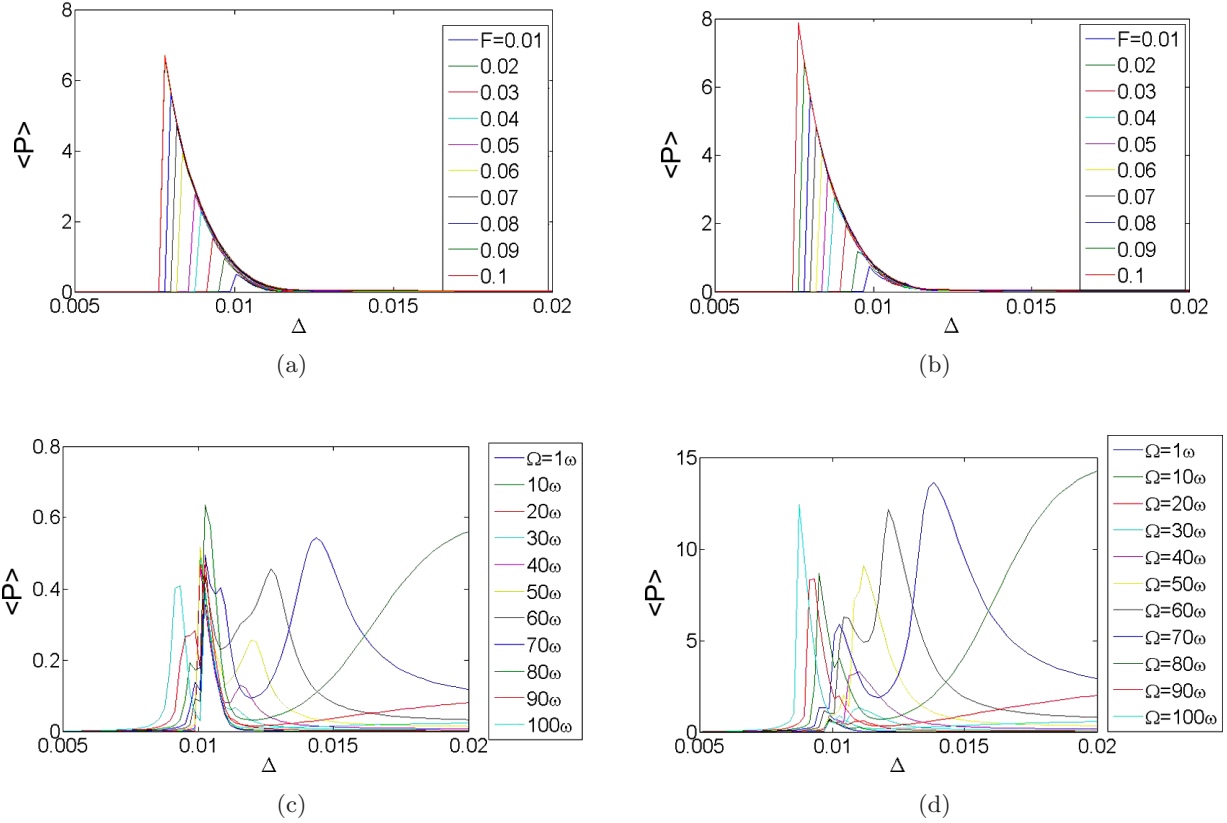


Fig. 9. Figures (a) and (b) plot the average electrical power $\langle P \rangle \propto \langle V^2 \rangle$ versus Δ , for $f = 0.1 \times 10^{-2}$ and $f = 0.5 \times 10^{-2}$ for different values of F . Figures (c) and (d) plot the average electrical power $\langle P \rangle$ versus Δ , for $f = 0.1 \times 10^{-2}$ and $f = 0.5 \times 10^{-2}$ for different values of the HF frequency Ω . The figures (a) and (b) show peaks in the generated electrical power $\langle P \rangle$ for the same values for which the VR occurs, as shown in Fig. 7. The figures (c) and (d) show that the behavior of the electrical power generated is largely affected by the value of Ω and we lose correlation with the Q factor figures, as we show in detail below. In all these curves, we have used $(x_0, y_0, v_0) = (0.001, 0, 0)$ as the initial condition.

$\Omega = 100\omega$, and for $\Delta = 0.001$ for lower frequencies, $\omega \leq \Omega \leq 50\omega$. Then, for $0.001 < \Delta < 0.013$ the maximum is reached by the curve $\Omega = 60\omega$, for $0.013 \leq \Delta \leq 0.016$ by the curve $\Omega = 70\omega$, and finally for $\Delta \geq 0.016$ by the curve $\Omega = 80\omega$. A discrepancy can be detected for $\Omega = 50\omega$, in fact

in Fig. 11(b) a higher peak detaches for a different value of Δ than in Fig. 10(b). Indeed, another difference is the scale of the average electrical power generated. We want to underline how the f value can be decisive in order to harvest more energy. We have generated all these figures with an initial

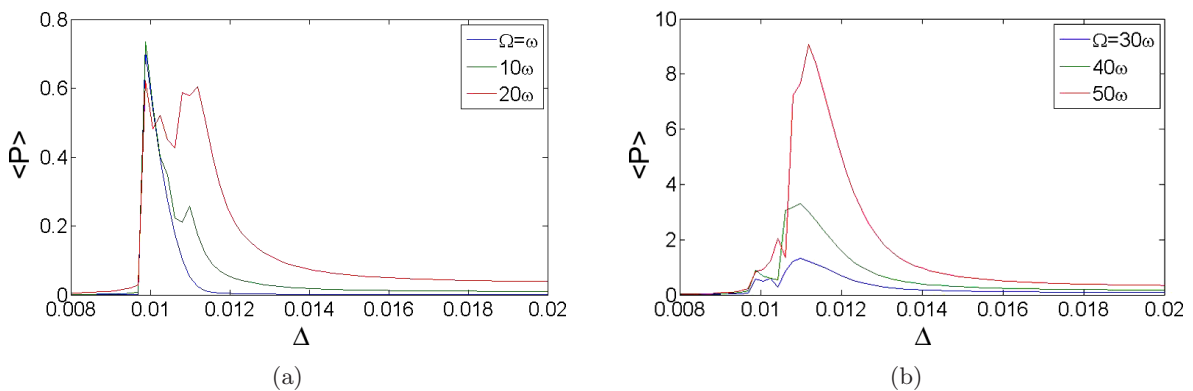


Fig. 10. Figures (a)–(d) show details of Fig. 9(c). We observe that the dependence of $\langle P \rangle$ on Δ takes larger values for frequencies Ω in the range $60 \leq \Omega/\omega \leq 80$.

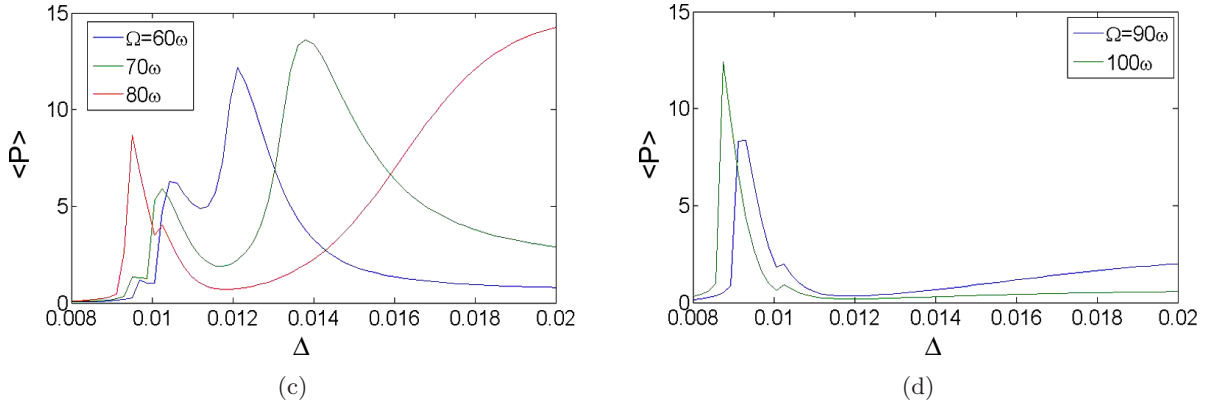


Fig. 10. (Continued)

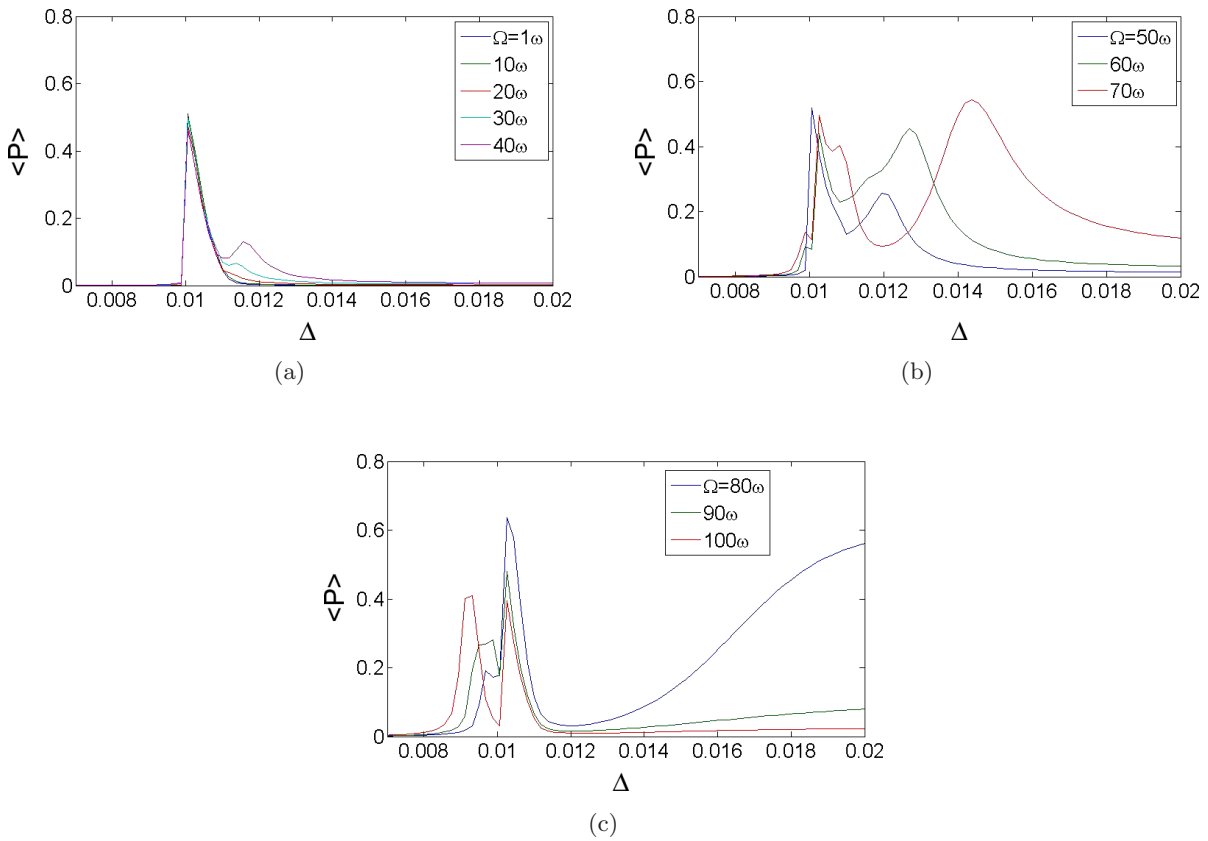


Fig. 11. Figures (a)–(c) show details of Fig. 9(d). In this case, the dependence of $\langle P \rangle$ on Δ takes larger values for frequencies Ω in the range $60 \leq \Omega/\omega \leq 90$.

condition $(x_0, \dot{x}_0, v_0) = (0.001, 0, 0)$. We have also studied the average electrical power generated by 300 different initial conditions, then we have calculated the mean value and plotted it in as a function of Δ . The figures generated were not only similar, but equal to the figures above. This tells us that the system has a strong robustness towards variations of the initial conditions.

4. Numerical Analysis of the Average Electrical Power of the System

After showing the response of the system as a function on the parameter Δ , we study the corresponding response as a function of both the forcing amplitude F/f and the frequency Ω/ω ratios since

these parameters are crucial in the energy harvested by the mechanical system.

In Figs. 12(a) and 12(b) it is possible to observe a maximum for $80 < \Omega/\omega < 100$, also in this case the magnitude of the peaks of the electrical power response is very different, due to the value of the HF forcing amplitude f . Figures 12(c)–12(e) show the electrical power response of the system for larger amplitudes where every curve is plotted for different Ω values. In Fig. 12(c) the response grows in an

oscillatory way and only for $F/f \geq 300$ the curve related to $\Omega = 80\omega$ detaches and indicates more generated electrical power than the others. On the other hand, in Fig. 12(d) we can see that for large values of F/f , the curve of $\Omega = 80\omega$ gives a higher response in the electrical power with respect to the others. But, if we take a look at Fig. 12(e), that is a zoom of the previous figure in the region $F/f < 100$, for values of the forcing $F/f < 50$, the maximum generated electrical power is given by the curve of

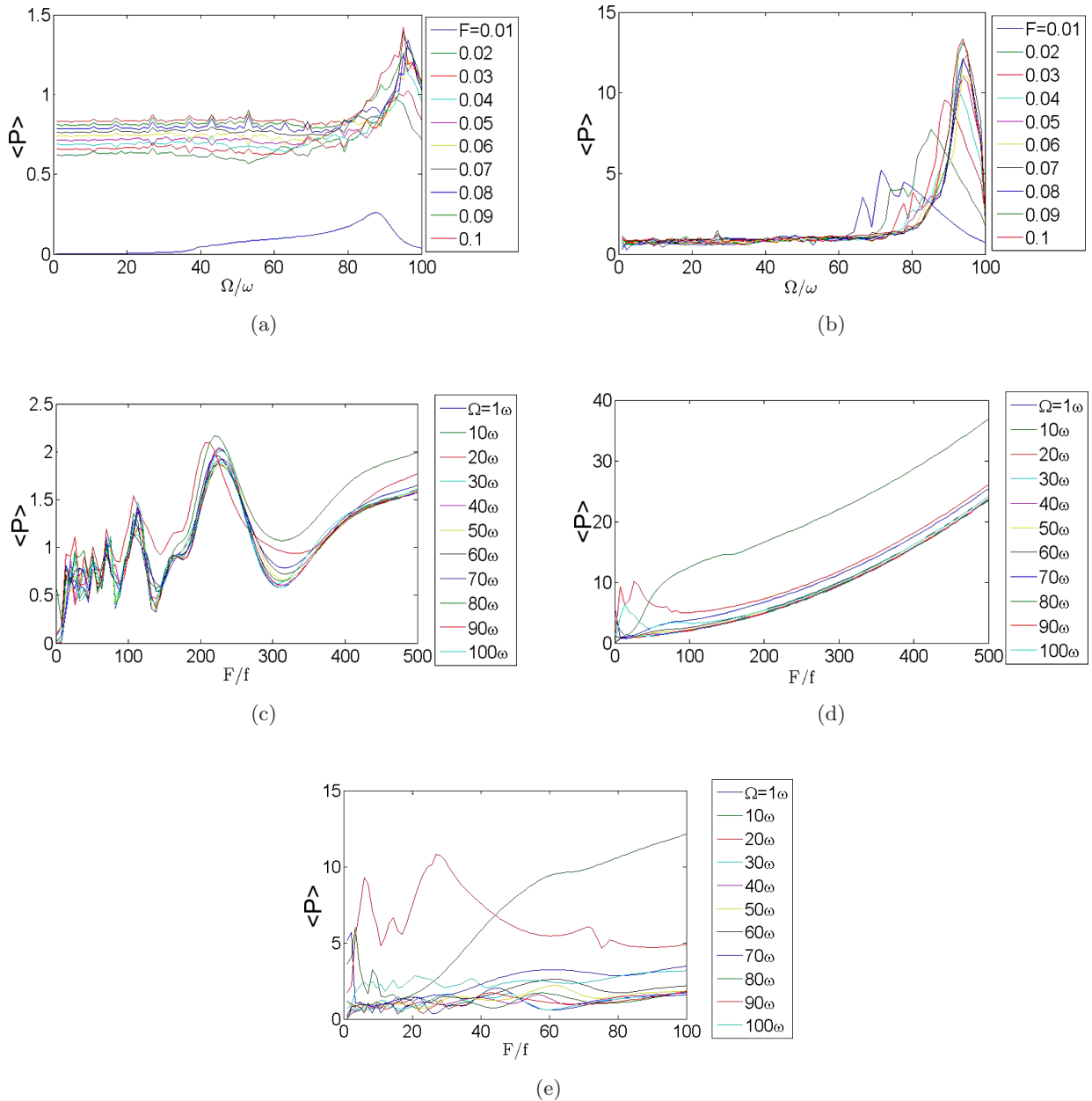


Fig. 12. Figures (a)–(e) show the average electrical power $\langle P \rangle \propto \langle V^2 \rangle$ versus the ratio Ω/ω and F/f . It is possible to see that in figures (a) and (b) we have a maximum for values of the HF frequency Ω in the range $80 \leq \Omega/\omega \leq 100$. In figures (c) and (d) we observe that a HF frequency value $\Omega = 80\omega$ detaches for higher values of the amplitude F . Figure (e) is a zoom of figure (d), in which the curve $\Omega = 90\omega$ gives the maximum electrical power for smaller values of the amplitudes.

$\Omega = 90\omega$. To summarize, the largest value of the response of the system takes place for $f = 0.5 \times 10^{-2}$ as we can easily observe in Figs. 12(b) and 12(d) where the maximum occurs for $\Omega = 80\omega$.

5. The Map of the Electrical Power Response of the System

We have seen in a previous section that an enhancement of the average electrical power generated by the system has taken place when the VR phenomenon occurs. Now, we explore this by using a (F, f) plot, which we call *forcing space*. For that purpose, we have carried out different simulations for three different values of Δ , while the other parameters do not change so that $\omega = 0.5$, $\Omega = 10\omega$ and $(x_0, \dot{x}_0, v_0) = (0.001, 0, 0)$. The figures that we have generated show a color gradient, from blue to red as a function of the electrical power, for different values of both HF and LF forcing amplitudes. In Figs. 12 and 14, even if the scale of the electrical power is different, a common pattern is observed. We can see that the higher the two forcing amplitudes, the higher the electrical power generated. However, we have a completely different pattern in Fig. 13, where more complicated structures are shown. It is possible to distinguish several red regions, that show us the values of the forcing amplitudes that allow us to harvest the maximum

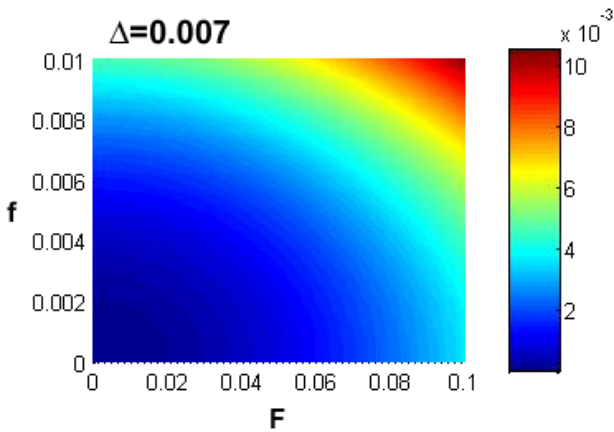


Fig. 13. The average electrical power $\langle P \rangle \propto \langle V^2 \rangle$ generated by the harvester for different values of the forcing amplitudes f, F for $\Delta = 0.007$. The color gradient indicates the amount of power generated as a function of the forcing amplitudes, from blue to red, from the smallest amount of electrical power to the highest respectively. It is possible to see that the bigger the two amplitudes, the bigger is the electrical power generated. We have used $(x_0, y_0, v_0) = (0.001, 0, 0)$ as the initial condition.

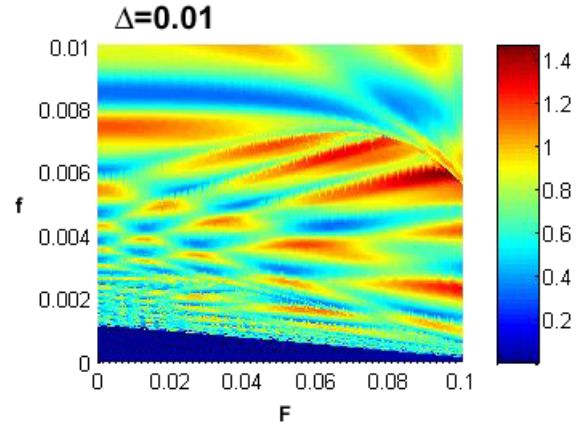


Fig. 14. The average electrical power $\langle P \rangle \propto \langle V^2 \rangle$ generated by the harvester for different values of the forcing amplitudes f, F for $\Delta = 0.01$. The color gradient indicates the amount of electrical power generated as a function of the forcing amplitudes, from blue to red, from the smallest amount of electrical power to the highest respectively. It is possible to see that some structures show up and we have regions of F, f values for which the electrical power is maximum. We have used $(x_0, y_0, v_0) = (0.001, 0, 0)$ as the initial condition.

electrical power. These regions are surrounded by yellow ones, in which the electrical power that we can harvest is smaller. Finally, we can observe some blue regions for very small forcing amplitudes f , where the electrical power generated is even smaller or almost zero. Note that the color gradient scale of Figs. 13–15 are very different. In Fig. 13, the

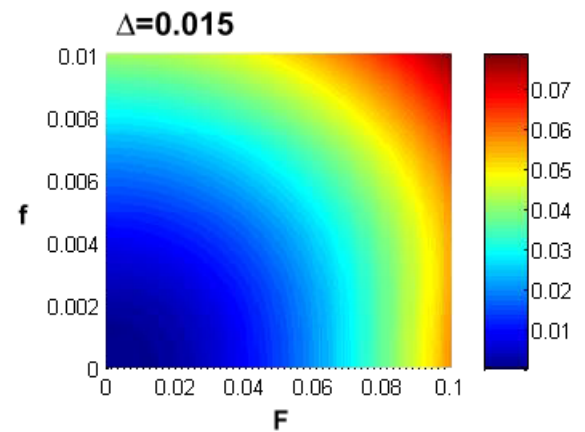


Fig. 15. The average electrical power $\langle P \rangle \propto \langle V^2 \rangle$ generated by the harvester for different values of the forcing amplitudes f, F for $\Delta = 0.015$. The color gradient indicates the amount of electrical power generated in function of the forcing amplitudes, from blue to red, from the smallest amount of electrical power to the highest respectively. It is possible to see that the bigger the two amplitudes, the bigger is the electrical power generated. We have used $(x_0, y_0, v_0) = (0.001, 0, 0)$ as the initial condition.

electrical power generated by the system is much higher than in the other cases. With the analysis of these last figures we have shown that for the case of $\Delta = 0.001$, an enhancement of the electrical power generated by the system appears. Besides, we can visualize as well the regions in the forcing space for which this occurs when the pattern is more clear. We think that these kinds of graphical tools might help experimentally to obtain an optimal enhancement of the average electrical power. We think that, this is crucial for a better understanding of the electrical power associated to different values of the forcing amplitudes. In fact, it gives us the opportunity to adjust the harvester to the environmental conditions in order to harvest the exact amount of energy that we need from the system.

6. Conclusions

In this work, we have studied a mechanical system which has been modeled as a bistable oscillator designed to harvest energy driven by a HF and a LF harmonic external forcing. We have shown how the distance between the magnets, Δ , may be crucial for the occurrence of the VR phenomenon, and as a matter of fact we have computed the values for which VR occurs. Then, we have related the VR with the optimal electrical power responses. We have also computed the average electrical power for small and large variations in the amplitudes and forcing frequencies. Furthermore, we have calculated the average electrical power $\langle P \rangle \propto V^2$ generated for different values of F and f where further information related to the different regions of the forcing space can be derived as the optimal situation for which the electrical power generated reaches its maximum and minimum. Some interesting patterns have been observed mainly for the case $\Delta = 0.001$. We think that this graphical study constitutes a useful tool to show for which values of the forcing amplitudes the electrical power generated is enhanced, as well as to gain a better knowledge about its prediction. To summarize, we believe that a complete study of this kind should present the possibility to set the harvester so that it can respond, maybe automatically, in the best way to the environmental conditions.

Acknowledgments

We acknowledge financial support from the Spanish Ministry of Economy and Competitiveness under

Project No. FIS2013-40653-P. M. Cocco acknowledges financial support for a research stay from the Universidad Rey Juan Carlos, under grant number PPR-2012-28, and the warm hospitality received at Lublin University of Technology, where part of this work was carried out. G. Litak was supported by the Polish National Science Center under the grant agreement No. 2012/05/B/ST8/00080.

References

- Anton, S. R. & Sodano, H. A. [2007] "A review of power harvesting using piezoelectric materials (2003–2006)," *Smart Mater. Struct.* **16**, 1.
- Arnold, D. P. [2007] "Review of microscale magnetic power generation," *IEEE Trans. Magn.* **43**, 3940.
- Blekhman, I. I. & Landa, P. S. [2004] "Conjugate resonances and bifurcations in nonlinear systems under biharmonic excitation," *Int. J. Nonlin. Mech.* **39**, 421.
- Borowiec, M., Rysak, A., Betts, D. H., Bowen, C. R., Kim, H. A. & Litak, G. [2014] "Complex response of the bistable laminated plate: Multiscale entropy analysis," *Eur. Phys. J. Plus* **129**, 211.
- Butcher, J. C. [1987] *The Numerical Analysis of Ordinary Differential Equations, Runge–Kutta and General Linear Methods* (Wiley, Chichester and NY).
- Cocco, M., Litak, G., Seoane, J. M. & Sanjuán, M. A. F. [2014] "Energy harvesting enhancement by vibrational resonance," *Int. J. Bifurcation and Chaos* **24**, 1430019-1–7.
- Cottone, F., Vocca, H. & Gammaitoni, L. [2009] "Nonlinear energy harvesting," *Phys. Rev. Lett.* **102**, 080601.
- Daza, A., Wagemakers, A., Rajasekar, S. & Sanjuán, M. A. F. [2013] "Vibrational resonance in a time-delayed genetic toggle switch," *Commun. Nonlin. Sci. Numer. Simulat.* **18**, 411–416.
- Deng, B., Wang, J. & Wei, X. [2009] "Effect of chemical synapse on vibrational resonance in coupled neurons," *Chaos* **19**, 013117.
- Friswell, M. I., Ali, S. F., Adhikari, S., Lees, A. W., Bilgen, O. & Litak, G. [2011] "Nonlinear piezoelectric vibration energy harvesting from an inverted cantilever beam with tip mass," *J. Intell. Mater. Syst. Struct.* **23**, 1505.
- Gammaitoni, L., Neri, I. & Vocca, H. [2009] "Nonlinear oscillation for vibrational energy harvesting," *Appl. Phys. Lett.* **94**, 164102.
- Gandhimathi, V. M., Rajasekar, S. & Kurths, J. [2006] "Vibrational and stochastic resonances in two coupled overdamped anharmonic oscillators," *Phys. Lett. A* **360**, 279–286.
- Gitterman, M. [2001] "Bistable oscillator driven by two periodic fields," *J. Phys. A: Math. Gen.* **34**, 355.

- Haris, P., Bowen, C. R. & Kim, H. A. [2014] “Manufacture and characterisation of piezoelectric broadband energy harvesters based on asymmetric bistable laminates,” *J. Multifunc. Compos.* **3**, 113.
- Harne, R. L. & Wang, K. W. [2013] “A review of the recent research on vibration energy harvesting via bistable systems,” *Smart Mater. Struct.* **22**, 023001.
- Jayakumari, S., Chinnathambi, V., Rajasekar, S. & Sanjuán, M. A. F. [2009] “Vibrational resonance in groundwater-dependent plant ecosystems,” *Chaos* **19**, 043128.
- Landa, P. S. & McClintock, P. V. E. [2000] “Vibrational resonance,” *J. Phys. A: Math. Gen.* **33**, 433–438.
- Litak, G., Friswell, M. I. & Adhikari, S. [2010] “Magnetopiezoelectric energy harvesting driven by random excitations,” *Appl. Phys. Lett.* **96**, 214103.
- Paradiso, J. A. & Starner, T. [2005] “Energy scavenging for mobile and wireless electronics,” *IEEE Pervasive Comput.* **4**, 18–27.
- Pellegrini, S. P., Tolou, N., Schenk, M. & Herder, J. L. [2012] “Bistable vibration energy harvesters: A review journal of intelligent material systems and structures,” *J. Intell. Mater. Syst. Struct.* **24**, 1303.
- Rajasekar, S., Abirami, K. & Sanjuán, M. A. F. [2011] “Novel vibrational resonance in multistable systems,” *Chaos* **21**, 033106.
- Roundy, S., Wright, P. K. & Rabaey, J. [2003] “A study of low level vibrations as a power source for wireless sensor nodes,” *Comput. Commun.* **26**, 1131–1144.
- The data and tables on the forcing amplitudes and frequencies can be found in: Department of Environment and Conservation [2006] “Assessing vibration: A technical guideline,” <http://www.environment.nsw.gov.au/resources/noise/vibrationguide0643.pdf>.
- Twiefel, J. & Westermann, H. [2013] “Survey on broadband techniques for vibration energy harvesting,” *J. Intell. Mater. Syst. Struct.* **24**, 1291.
- Vocca, H., Travasso, F., Neri, I. & Gammaitoni, L. [2012] “Kinetic energy harvesting with bistable oscillators,” *Appl. Energ.* **97**, 771.
- Zaikin, A. A., López, L., Baltanás, J. P., Kurths, J. & Sanjuán, M. A. F. [2002] “Vibrational resonance in noise induced structures,” *Phys. Rev. E* **66**, 011106.